Front. Optoelectron. 2012, 5(4): 445–456
DOI 10.1007/s12200-012-0288-4

RESEARCH ARTICLE

Homogeneous and inhomogeneous broadening effects on static and dynamic responses of quantum-dot semiconductor optical amplifiers

Hussein TALEB, Kambiz ABEDI (✉)

Department of Electrical Engineering, Faculty of Electrical and Computer Engineering, Shahid Beheshti University, Tehran 1983963113, Iran

Abstract In this paper, the effects of homogeneous and inhomogeneous broadenings on the response of quantum-dot semiconductor optical amplifier (QD-SOAs) are investigated. For the first time, the state space model is used to simulate static and dynamic characteristics of the QD-SOA. It is found that with decreasing the homogeneous and inhomogeneous broadenings, the saturation power of the QD-SOA decreases and the optical gain and the ultrafast gain compression increase. Simulation results show that with decreasing the homogeneous broadening from 20 to 1 meV, the gain compression increases from 40% to 90%, the unsaturated optical gain becomes approximately tripled, and the saturation power becomes two times less. Also, simulations demonstrate that with decreasing the inhomogeneous broadening from 50 to 25 meV, the gain compression increases from less than 50% to more than 90%, the unsaturated optical gain becomes approximately 10-fold, and the saturation power becomes three times less. In addition, it is found that the homogeneous and inhomogeneous linewidths should be small for nonlinear applications. The homogeneous and inhomogeneous broadenings need to be large enough for linear applications.

Keywords homogeneous broadening, inhomogeneous broadening, quantum-dot (QD), semiconductor optical amplifier (SOA)

1 Introduction

In recent years, quantum-dot (QD) based optoelectronic devices, like QD-lasers and quantum-dot semiconductor optical amplifier (QD-SOAs), have directed the attention of many researchers. Both theoretical and experimental studies have demonstrated unique feature of these devices for use in all optical signal processing and optical communication systems. Ultra-fast gain response [1–4], low noise figure [5], high saturation power [6], ultra-wide gain bandwidth [7,8], high temperature stability [9], and capability of operation at terabit per second speeds in presence of a control signal [10], are the most important features of QD-SOAs.

The inhomogeneous broadening of the gain spectrum is a result of the fluctuations in the size of self-assembled QDs, which leads to a large gain bandwidth for QD-SOAs [11]. However, with increasing the inhomogeneous broadening, the modal gain at all wavelengths in the gain bandwidth decreases [12]. Also, since the light–dot interaction occurs over a finite time period, the gain is homogeneously broadened. Thus, the inhomogeneously broadened gain spectrum consists of groups of homogeneously broadened subgroups of QDs of different size and consequently different transition energies [11]. Homogeneous broadening of the optical gain makes the static and dynamic characteristics of QD-SOAs dependent on the ambient temperature and physical parameters of semiconductor QDs. Because of the importance of this subject, the objective in this paper is to find out the improvements which can be obtained through reduction or increase of the homogeneous and inhomogeneous broadenings. For this purpose, using the state space model of QD-SOAs, we evaluate the static and dynamic responses of a typical QD-SOA under different values of the homogeneous and inhomogeneous broadenings. Then the simulation results are analyzed in details.

2 State space model of QD-SOAs

The device is an InAs/GaAs QD-SOA, which operates around 1.3 μm. A 10-fold stacked QD active region is

Received September 5, 2012; accepted October 16, 2012

E-mail: K_Abedi@sbu.ac.ir

sandwiched between two AlGaAs cladding layers. InAs QDs in each layer are grown by the Stranski-Krastanow growth mode and are covered with a 5-nm-thick InGaAs capping layer. Also, QD layers are separated by 33-nm-thick p-doped GaAs spacer layers [4]. Since QDs are grown self-assembly, they have slightly different properties induced by the size fluctuations. It is assumed that QDs have a Gaussian size distribution and consist of 181 spectral groups, where all QDs in each group are identical and energy separation between two adjacent groups is ΔE = 1 meV. The energy band diagram of a QD group is illustrated in Fig. 1, where the relative energy positions of the most probable group are designated in the figure. As can be seen in the figure, each QD group has three energy levels in the conduction band (CB) and three energy levels in the valence band (VB). To model the effect of the carrier reservoir, a many-fold degenerate quantum well (QW) state is considered in the band diagram. To evaluate the dynamics of carriers and photons in QD-SOA cavity, a state space model for the QD-SOA is developed. The state space model of the QD-SOA is based on rate equation model, which was proposed by Kim et al. [4,12]. The essence of the state space model of the QD-SOA can be summarized as follows [13]. Since, the photon density along the QD-SOA cavity is a function of distance and time, the carrier density is also a function of distance and time. However, it is shown that the optical gain of the QD-SOA is weakly dependent on the distribution of the carriers along the cavity [14]. Thus, we can assume that the carrier density along the QD-SOA cavity is completely uniform and does not have any variation. This assumption enables us to derive the state space model for the QD-SOA, where the average values of carrier occupation probabilities are the state variables of the system.

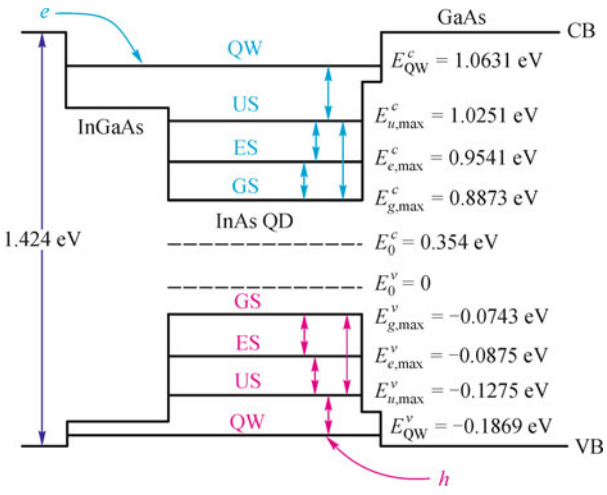

Fig. 1 Energy band diagram of QD group. Relative energies of 91-th QD group are indicated in the figure. QW: quantum well, US: upper state, ES: excited state, GS: ground state

Self-assembled QDs have three energy states in the CB and three energy states in the VB, which are known as the GS, the ES, and the US. Thus, the carrier dynamics in each QD group is described by six state variables. So, the QD ensemble can be described by 1086 state variables (6 × 181). Considering the QW state in the CB and VB, the QD-SOA can be described by a nonlinear state space model with 1088 state variables. Based on the rate equation model presented in Refs. [4,12], the state update equations of the QD-SOA read as follows.

$$\frac{\mathrm{d}f_w^{c(v)}}{\mathrm{d}t} = \frac{JA}{qN_W^{c(v)}} - \frac{\sqrt{f_w^c f_w^v}}{\hat{\tau}_{wr}^{c(v)}} + \frac{D_u^{c(v)}}{D_w^{c(v)}} \sum_{j=1}^{2M+1} G_j^{c(v)} \left(\frac{f_{u,j}^{c(v)}}{\hat{\tau}_{uw,j}^{c(v)}} \left(1 - f_w^{c(v)}\right) - \frac{f_w^{c(v)}}{\hat{\tau}_{wu}^{c(v)}} \left(1 - f_{u,j}^{c(v)}\right) \right), \tag{1a}$$

$$\begin{aligned} \frac{\mathrm{d}f_{u,j}^{c(v)}}{\mathrm{d}t} = & \frac{f_w^{c(v)}}{\hat{\tau}_{wu}^{c(v)}} \left(1 - f_{u,j}^{c(v)}\right) - \frac{f_{u,j}^{c(v)}}{\hat{\tau}_{uw,j}^{c(v)}} \left(1 - f_w^{c(v)}\right) + \frac{D_e^{c(v)}}{D_u^{c(v)}} \left(\frac{f_{e,j}^{c(v)}}{\hat{\tau}_{eu}^{c(v)}} \left(1 - f_{u,j}^{c(v)}\right) - \frac{f_{u,j}^{c(v)}}{\hat{\tau}_{ue}^{c(v)}} \left(1 - f_{e,j}^{c(v)}\right) \right) \\ & + \frac{D_g^{c(v)}}{D_u^{c(v)}} \left(\frac{f_{g,j}^{c(v)}}{\hat{\tau}_{gu}^{c(v)}} \left(1 - f_{u,j}^{c(v)}\right) - \frac{f_{u,j}^{c(v)}}{\hat{\tau}_{ug}^{c(v)}} \left(1 - f_{g,j}^{c(v)}\right) \right) - \frac{\sqrt{f_{u,j}^c f_{u,j}^v}}{\hat{\tau}_{ur}^{c(v)}}, \end{aligned} \tag{1b}$$

$$\begin{aligned} \frac{\mathrm{d}f_{e,j}^{c(v)}}{\mathrm{d}t} = & \frac{f_{u,j}^{c(v)}}{\hat{\tau}_{ue}^{c(v)}} \left(1 - f_{e,j}^{c(v)}\right) - \frac{f_{e,j}^{c(v)}}{\hat{\tau}_{eu}^{c(v)}} \left(1 - f_{u,j}^{c(v)}\right) + \frac{D_g^{c(v)}}{D_e^{c(v)}} \left(\frac{f_{g,j}^{c(v)}}{\hat{\tau}_{ge}^{c(v)}} \left(1 - f_{e,j}^{c(v)}\right) - \frac{f_{e,j}^{c(v)}}{\hat{\tau}_{eg}^{c(v)}} \left(1 - f_{g,j}^{c(v)}\right) \right) \\ & - \frac{\sqrt{f_{e,j}^c f_{e,j}^v}}{\hat{\tau}_{dr}} - \frac{\Gamma}{N_{E,j}^{c(v)}} \sum_k \frac{P_{k,in} g_{jk}^e \left[e^{([\Gamma g(t,\omega_k) - \alpha_i] L_{ca})} - 1 \right]}{E_k [\Gamma g(t,\omega_k) - \alpha_i]} (f_{e,j}^c + f_{e,j}^v - 1), \end{aligned} \tag{1c}$$

$$\frac{\mathrm{d}f_{g,j}^{c(v)}}{\mathrm{d}t} = \frac{f_{u,j}^{c(v)}}{\hat{\tau}_{ug}^{c(v)}}\left(1-f_{g,j}^{c(v)}\right)-\frac{f_{g,j}^{c(v)}}{\hat{\tau}_{gu}^{c(v)}}\left(1-f_{u,j}^{c(v)}\right) + \frac{f_{e,j}^{c(v)}}{\hat{\tau}_{eg}^{c(v)}}\left(1-f_{g,j}^{c(v)}\right)-\frac{f_{g,j}^{c(v)}}{\hat{\tau}_{ge}^{c(v)}}\left(1-f_{e,j}^{c(v)}\right)-\frac{\sqrt{f_{g,j}^{c}f_{g,j}^{v}}}{\hat{\tau}_{dr}} - \frac{\Gamma}{N_{G,j}^{c(v)}}\sum_{k}\frac{P_{k,in}g_{jk}^{g}\left[e^{([\Gamma g(t,\omega_k)-\alpha_i]L_{ca})}-1\right]}{E_k[\Gamma g(t,\omega_k)-\alpha_i]}(f_{g,j}^{c}+f_{g,j}^{v}-1). \tag{1d}$$

In Eqs. (1a)–(1d), $f_{g,j}^{c(v)}$, $f_{e,j}^{c(v)}$, $f_{u,j}^{c(v)}$, and $f_{w}^{c(v)}$ are the state variables of the system. For instant, $f_{g,j}^{c(v)}$ signifies the state variable associated to the GS of the j-th QD group in the conduction (valence) band. In the following, the parameters of the state space model are described in details.

In Eq. (1a), the term $I = JA$ is the injected current, where J is the injection current density, q is the electron charge. $A = WL_{ca}$ is the area of the active region, where W and L_{ca} are the width and length of the active region, respectively. The maximum allowable carrier numbers in the QW state is given by [15]

$$N_{W}^{c(v)} = N_{QD}D_{w}^{c(v)}. \tag{2}$$

The maximum allowable carrier numbers at the j-th group of the GS, the ES, and the US are respectively given by [12]

$$N_{G,j}^{c(v)} = N_{QD}D_{g}^{c(v)}G_{j}^{c(v)}, \tag{3a}$$

$$N_{E,j}^{c(v)} = N_{QD}D_{e}^{c(v)}G_{j}^{c(v)}, \tag{3b}$$

$$N_{U,j}^{c(v)} = N_{QD}D_{u}^{c(v)}G_{j}^{c(v)}. \tag{3c}$$

In Eqs. (2) and (3), $N_{QD} = l_D n_D A$ is the total number of QDs, where n_D is the QD surface density and l_D is the number of QD layers. $D_{g}^{c(v)}$, $D_{e}^{c(v)}$, $D_{u}^{c(v)}$ and $D_{w}^{c(v)}$ are respectively the degeneracy (including the spin) of the GS, the ES, the US and the QW state in the conduction (valence) band. In Eq. (1a), the term $G_{j}^{c(v)}$ is the fraction of the j-th QD group among the inhomogeneously broadened electron (hole) states. The inhomogeneous broadening for the GS, the ES, and the US are given by the following Gaussian line shape functions [12]:

$$G_{j}^{c(v)} = \frac{1}{\sqrt{2\pi\sigma_{in,c(v)}^{2}}}\exp\left[-\frac{\left(E_{g,j}^{c(v)}-E_{g,\max}^{c(v)}\right)^{2}}{2\sigma_{in,c(v)}^{2}}\right] \times r_{c(v)}\Delta E, \tag{4a}$$

where

$$E_{g(e,u),j}^{c} = E_{g(e,u),\max}^{c} + [j-(M+1)] \times r_{c}\Delta E, \tag{4b}$$

$$E_{g(e,u),j}^{v} = E_{g(e,u),\max}^{v} - [j-(M+1)] \times r_{v}\Delta E. \tag{4c}$$

The term $\sigma_{in,c(v)} = \Gamma_{ih}^{c(v)}/2.356$ is the variance of the inhomogeneous QD electron (hole) distribution, where $\Gamma_{ih}^{c(v)}$ represents the FWHM of the inhomogeneously broadened electron (hole) states. The terms $E_{g(e,u),j}^{c}$ and $E_{g(e,u),j}^{v}$ are the confined GS (ES, US) energy of the j-th QD group for electrons and holes, respectively. Also, the terms $E_{g(e,u),\max}^{c}$ and $E_{g(e,u),\max}^{v}$ are the relative energy positions of the electron and hole states in the most probable QD group (91-th QD group). In Eqs. (1c) and (1d), $P_{k,in}$ and $E_k = \hbar\omega_k$ are the input optical power and the energy of the k-th photon mode, and the term Γ is the optical confinement factor. In Eqs. (1c) and (1d), the linear material gain at frequency ω_k is given by [16]

$$g(t,\omega_k) = \sum_{\ell=g,e}\sum_{j=1}^{2M+1} g_{jk}^{\ell}(\omega_k)[f_{\ell,j}^{c}+f_{\ell,j}^{v}-1], \tag{5a}$$

where the linear optical gain that the GS (ES) of the j-th QD group gives to the k-th photon mode is expressed as [12]

$$g_{jk}^{g(e)}(\omega_k) = \frac{\pi\hbar q^2 N_D D_{g(e)}}{cn_r\varepsilon_0 m_0^2 E_k}|M_{\mathrm{env}}|^2\left\langle|\hat{e}.\mathbf{p}_{cv}|^2\right\rangle L_{j}^{g(e)}G_{j}^{s}. \tag{5b}$$

The term $L_{j}^{g(e)}$ is the homogeneous broadening function with a Lorentzian shape

$$L_{j}^{g(e)} = \frac{1}{\pi}\frac{\Gamma_h/2}{\left(E_{g(e),j}^{s}-E_k\right)^{2}+(\Gamma_h/2)^{2}}. \tag{5c}$$

The Lorentzian lineshape is arisen from exponential time dependence of the decay of the polarization. The term G_{j}^{s} is the fraction of the radiative recombination of the j-th QD group

$$G_{j}^{s} = \frac{1}{\sqrt{2\pi\sigma_{in,s}^{2}}}\exp\left[-\frac{(E_{g,j}^{s}-E_{g,\max}^{s})^{2}}{2\sigma_{in,s}^{2}}\right]\Delta E, \tag{5d}$$

where the optical transition energy of the j-th QD group is given by [12]

$$E_{g(e),j}^{s} = E_{g(e),j}^{c}-E_{g(e),j}^{v}. \tag{5e}$$

In Eq. (5b), the term $\left\langle|\hat{e}.\mathbf{p}_{cv}|^2\right\rangle$ is the bulk momentum matrix element. $\left\langle|\hat{e}.\mathbf{p}_{cv}|^2\right\rangle = (m_0/6)E_p$, where m_0 is the free electron mass and E_p represents the optical matrix energy parameter. The term $|M_{\mathrm{env}}|^2$ represents the envelope function overlap between the QD electron and hole states,

c is the speed of light in free space, ε_0 is the vacuum permittivity, n_r is the refractive index of the material, $\hbar$ is reduced Planck constant, N_D is the volume density of self-assembled QDs which is related to the surface density via $N_D = n_D/L_H$ [17], where L_H is the height of one QD layer, and the volume of the active region is given by $V_d = l_D A L_H$. The time constants in the state space model read as follows. The effective value of electron (hole) relaxation lifetime from the InGaAs QW to the US ($\hat{\tau}_{wu}^{c(v)}$), from the US to the ES ($\hat{\tau}_{ue}^{c(v)}$), from the US to the GS ($\hat{\tau}_{ug}^{c(v)}$), and from the ES to the GS ($\hat{\tau}_{eg}^{c(v)}$). The relation between relaxation and excitation lifetimes is dictated by the principle of detailed balance [4]:

$$\hat{\tau}_{ge(gu,eu)}^{c} = \hat{\tau}_{eg(ug,ue)}^{c} \exp\left(\frac{\Delta E_{eg(ug,ue)}^{c}}{k_B T}\right), \tag{6a}$$

$$\hat{\tau}_{ge(gu,eu)}^{v} = f_D \hat{\tau}_{eg(ug,ue)}^{v} \exp\left(\frac{\Delta E_{eg(ug,ue)}^{v}}{k_B T}\right), \tag{6b}$$

where k_B is the Boltzmann's constant, T is the absolute temperature. The term f_D represents the doping factor which models the enhanced hole concentration in p-doped QDs, the terms $\Delta E_{eg}^{c(v)}$, $\Delta E_{ug}^{c(v)}$ and $\Delta E_{ue}^{c(v)}$ respectively represent the energy separation between the GS and the ES in the conduction (valence) band, between the GS and the US, and between the ES and the US.

$$\Delta E_{eg}^{c(v)} = \left| E_{g,\max}^{c(v)} - E_{e,\max}^{c(v)} \right|, \tag{7a}$$

$$\Delta E_{ug}^{c(v)} = \left| E_{g,\max}^{c(v)} - E_{u,\max}^{c(v)} \right|, \tag{7b}$$

$$\Delta E_{ue}^{c(v)} = \left| E_{e,\max}^{c(v)} - E_{u,\max}^{c(v)} \right|. \tag{7c}$$

Similarly

$$\hat{\tau}_{uw,j}^{c} = \hat{\tau}_{wu}^{c} \exp\left(\frac{\Delta E_{wu,j}^{c}}{k_B T}\right), \tag{8a}$$

$$\hat{\tau}_{uw,j}^{v} = f_D \hat{\tau}_{wu}^{v} \exp\left(\frac{\Delta E_{wu,j}^{v}}{k_B T}\right), \tag{8b}$$

where the term $\Delta E_{wu,j}^{c(v)} = \left| E_{QW}^{c(v)} - E_{u,j}^{c(v)} \right|$ is the energy separation between the ES of the j-th QD group and the QW state. The simulation parameters can be found in Table 1, unless otherwise specified [4,12,17].

3 Effects of homogeneous broadening on static and dynamic responses of QD-SOAs

Both theoretical and experimental studies have proven that the gain spectrum about the discrete energy levels of QDs is homogeneously broadened. This broadening is arisen from the fact that the interaction between light and QDs occurs over a finite period of time [18]. The homogeneous linewidth depends on variety factors, such as the temperature of the active region, the injection current density, the doping density, and the size distribution of QDs [18,19]. Homogeneous linewidth may be increased through increasing the injection current density or use of p-doped QDs in the spacer layer. Also, it decreases with decreasing the temperature. The temperature dependency of the homogeneous broadening is determined by considering the contributions of the acoustic phonons, the optical phonons as well as the zero-temperature lattice motion to the dephasing time [20]. The full width at half maximum (FWHM) of the homogeneous broadening (homogeneous linewidth) is related to the dephasing time via the relation $\Gamma_h = 2\hbar/\tau_h$ [12], where τ_h represents the dephasing time which can be described as a function of temperature [20]

$$\tau_h^{-1}(T) = \hat{\tau}_{dr}^{-1} + a.T + \frac{b}{\exp(E_a/k_B T) - 1}. \tag{9a}$$

Thus, the homogeneous broadening function can be expressed as a function of temperature

$$L_j^{g(e)}(T) = \frac{1}{\pi} \frac{\hbar \tau_h^{-1}(T)}{\left(E_{g(e),j}^{s}(T) - E_k\right)^2 + \left(\hbar \tau_h^{-1}(T)\right)^2}. \tag{9b}$$

Figure 2 represents the calculated homogeneous linewidth for temperatures between 0 and 400 K. From the figure, we can see that for temperatures beyond 150 K the homogeneous linewidth increase linearly with temperature with slope of 48 μeV/K. In Fig. 3(a), Lorentzian homogeneous broadening function plotted as a function of the photon energy for three different homogeneous linewidths. In Figs. 3(b) and 3(c), the term $L_j^g G_j^s$, which is proportional to the modal gain relevant to each QD group, is calculated for different homogeneous linewidths. In these subfigures, only a few numbers of homogeneous broadening functions are plotted. We can see that with increasing the homogeneous broadening, which can be caused by increasing the temperature of the active region due to significant contribution of acoustic phonons to the dephasing processes, the overlap integral between modal gains of different QD groups increases and a strong interaction between QDs occurs. On the other hand, with decreasing temperature and consequently the homogeneous linewidth, the interaction between different QDs decreases and QD groups tend to operate independently.

To investigate the effect of the homogeneous linewidth on dynamic characteristics of the QD-SOA, in the first step we investigate the carrier capturing into empty QD states. For this purpose, we assume that all QD states are initially empty. At t = 0, the pump source is switched on and a pump current with a density of J = 12 kA/cm^2 is injected

Table 1 Parameters used in numerical simulations

symbol	value	symbol	value
L_{ca}	2 mm	E_p	22.2 eV^{-1}
W	4 μm	$\Gamma_{ih}^{c(v)}$	40(10) meV
A	8×10^{-5} cm^2	Γ_{ih}	50 meV
L_H	5 nm	Γ_h	10 meV
l_D	10	Γ	0.025
α_i	5 cm^{-1}	$\hat{\tau}_{eg}^{c(v)}$	0.5(0.075) ps
T	300 K	$\hat{\tau}_{ug}^{c(v)}$	0.33(0.022) ps
n_D	5×10^{10} cm^{-2}	$\hat{\tau}_{ue}^{c(v)}$	0.66(0.043) ps
$D_g^{c,v}$	2	$\hat{\tau}_{wu}^{c(v)}$	1.8(0.078) ps
$D_e^{c,v}$	4	$\hat{\tau}_{dr}$	1 ns
$D_u^{c(v)}$	10(20)	$\hat{\tau}_{wr}^{c(v)}$	0.14(0.28) ns
$D_w^{c(v)}$	100(200)	$\hat{\tau}_{ur}^{c(v)}$	0.71(1.42) ns
$\lvert M_{\text{env}}\rvert^2$	0.88	$r_{c(v)}$	0.8(0.2)
$\langle \lvert \hat{e}.\mathbf{p}_{cv}\rvert^2 \rangle$	3.37×10^{-30} kg·eV	$2M+1$	181
f_D	6	n_r	3.51
N_D	10^{23} m^{-3}	V_d	4×10^{-10} cm^3

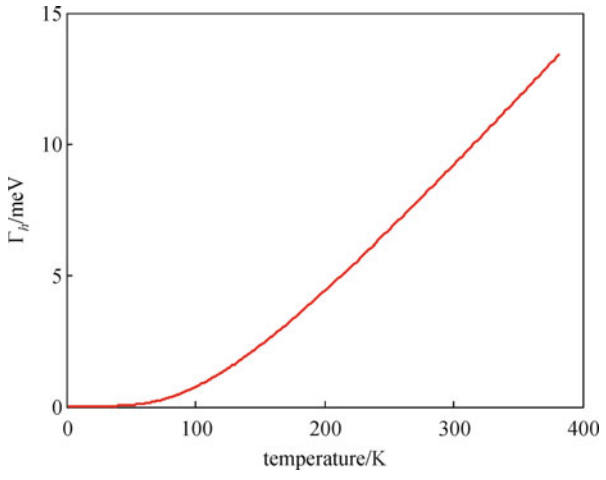

Fig. 2 Temperature dependence of homogeneous linewidth

into the active region of the QD-SOA. Then, at $t = 100$ ps, a continuous-wave (CW) optical signal corresponding to the GS transition is injected into the active region and the time response of the QD-SOA is monitored. Simulation results are presented in Fig. 4, where the dynamic response of the QD-SOA is evaluated under different values for the homogeneous broadening. As can be seen in Fig. 4, the GS steady-state is reached after 40 ps in all three plots. Also, as seen in the figure, the spectral width of the gain spectrum is decreased with decreasing the magnitude of the homogeneous broadening. However, since this reduction is not significant, we can say that the homogeneous broadening does not have a significant effect on the gain bandwidth. On the contrary, the modal gain is strongly dependent on the homogeneous broadening, where we can see that the gain peak can be greatly enhanced through decreasing the homogeneous linewidth. For instant, it can be seen form the figure that the GS and ES gain peaks will be reduced to half with increasing the homogeneous linewidth from 1 to 20 meV. Entering the CW signal into the active region at $t = 100$ ps leaves a spectral hole in the gain spectra, which is attributed to the carrier depletion around the resonant energy. The width of this spectral hole relates to the carrier–carrier scattering via homogeneous broadening and is deeper and narrower for smaller homogeneous linewidths [21]. As a result, the gain compression increase with decreasing the homogeneous broadenings, but the spectral width of the gain spectrum and the carrier capture rates are not significantly affected.

To study the effect of the homogeneous linewidth on the gain response of QD-SOAs, we numerically perform a single pulse pump-probe experiment, where we inject a Gaussian shaped optical pulse into the active region and monitor the gain dynamics of the QD-SOA. Simulation results are presented in Fig. 5. The energy of input photons is corresponding to the GS of 91-th QD group. The pulse width and energy of the input pulse are 0.5 ps and 0.75 pJ, respectively. The pulse is injected at $t = 3$ ps.

As can be seen in Figs. 5(a) and 5(b), the optical pulse depletes the GS carriers and leads to a reduction in the optical gain. Then, the GS is refilled mainly via the intra-dot relaxation of charge carriers from QD ESs and the gain is recovered within a few picoseconds. A comparison between Figs. 5(a) and 5(b) demonstrates that the optical gain and the gain compression can be greatly enhanced through reducing the homogeneous linewidth. For instant, Fig. 5(c) demonstrates that with decreasing the homogeneous broadening from 20 to 1 meV, the gain compression is increased from 40% to 90%, and the unsaturated optical gain is approximately tripled (it is increased from 9 to 14 dB). This behavior can be explained as follows. The QD-SOA contains many QD groups. However, some groups in the ensemble can contribute to amplification of the injected optical pulse. During the amplification of an optical pulse, a fraction of QD groups, where their transitions are in resonance with the pulse wavelength, interactes with propagating photons and will be strongly depleted. Once the magnitude of the homogeneous broadening decreases, the number of QD groups that contribute to the amplification of the input pulse decreases. As a result, a pronounced hole burning occurs at the energy of the input photons and the gain compression becomes significant. On the contrary, since in a gain media with a high homogeneous broadening a larger number of QD groups participate to the amplification process, the gain compression becomes smaller. Comparison between Figs. 5(a) and 5(b) also reveals that the ultrafast gain recovery time is approximately independent of magnitude

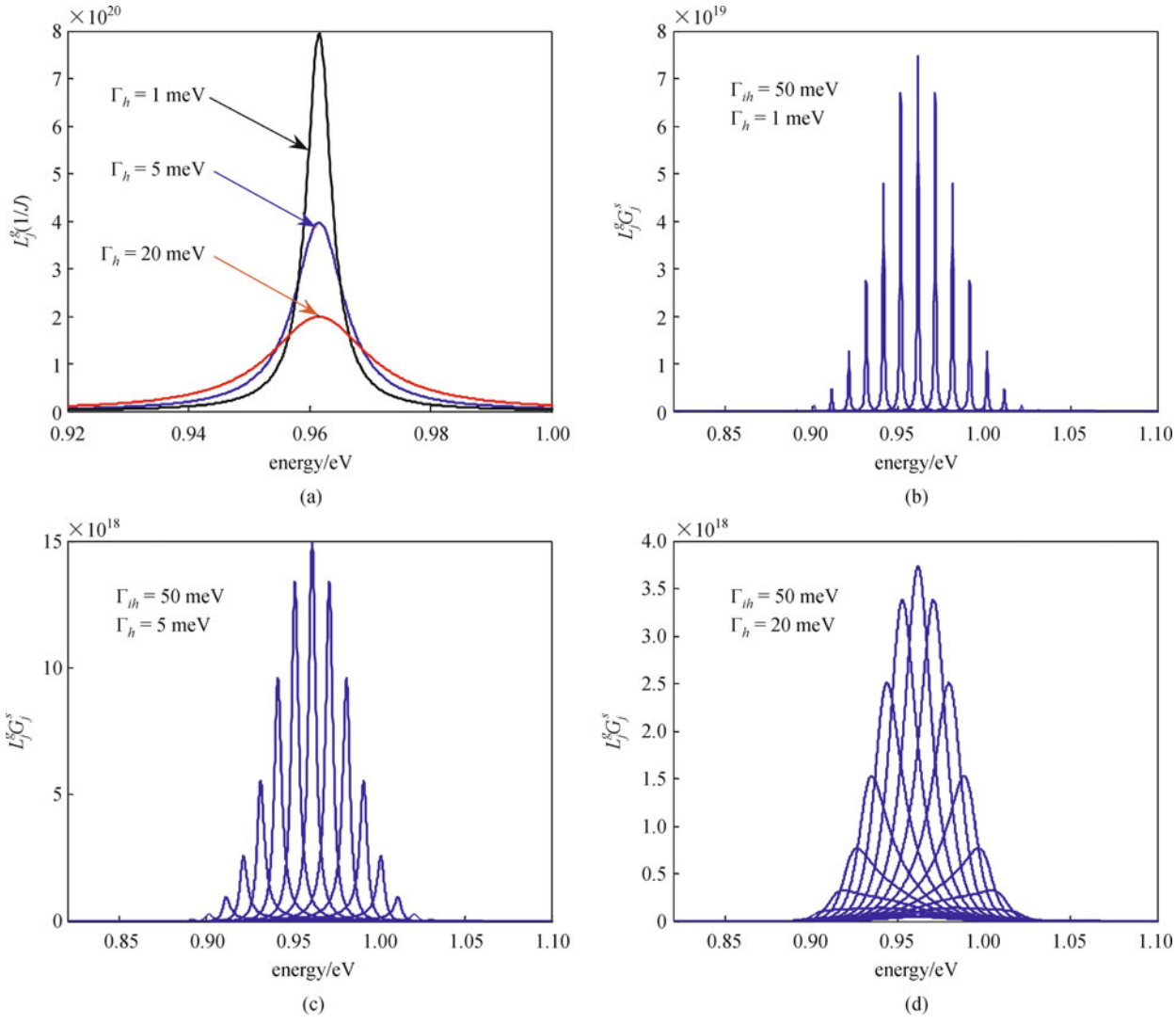

Fig. 3 (a) Homogenous broadening function calculated for different homogeneous linewidths. The product of homogeneous and inhomogeneous functions ($L_j^g G_j^s$) for different homogeneous linewidths, (b) $\Gamma_h = 1$ meV, (c) $\Gamma_h = 5$ meV and (d) $\Gamma_h = 20$ meV. The inhomogeneous linewidth is $\Gamma_{ih} = 50$ meV

of the homogeneous broadening. This is due to the fact that the ultrafast gain recovery is determined mainly by the carrier–carrier scattering processes, which are mainly determined by the injection current density.

Another important result of Fig. 5 is that the strength of the gain saturation is dependent on both homogeneous linewidth as well as injection current density. At relatively low current densities, i.e., $J = 2$ kA/cm^2, injection of the optical pulse leads to depletion of higher energy states that work as a carrier reservoir for the GS. Consequently, a wide-ranging saturation is occurred in the gain spectra. On the other hand, at high current densities, i.e., $J = 6$ kA/cm^2 and $J = 12$ kA/cm^2, injection of the optical pulse leads to depletion of the GS of QDs that are in resonance with the pulse wavelength and consequently a narrow-band saturation is occurred in the gain spectra (see Fig. 4). This is due to the fact that at high current densities, the higher energy states fill up quicker. Therefore, the gain compression decreases as the applied current or the homogeneous linewidth increase. Since the occupation of higher states is relatively unchanged at high current densities, spectral hole burning (SHB) will be the dominant gain saturation mechanism. Figure 5(c) represents the percentage gain compression as a function of the injection current density for different homogeneous linewidths. As seen in the figure, the gain compression reduces with increasing the injection current density. However, for smaller values of the homogeneous broadenings, this reduction is negligible. In other words, the gain compression is independent of the injected current if the homogeneous broadening is approximately less than 2 meV. This is due to the fact that the role of SHB as the gain saturation mechanism is more pronounced for smaller homogeneous broadenings. This result is important for nonlinear signal processing

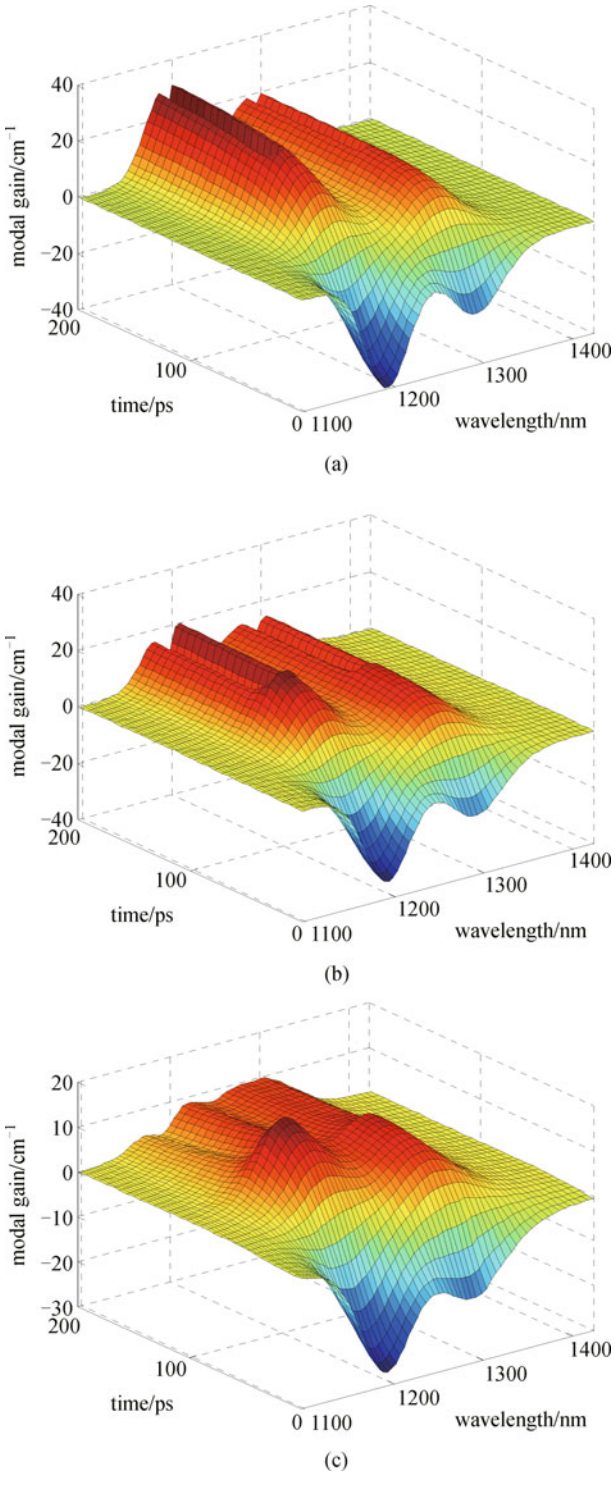

Fig. 4 Absorption/gain spectra of QD-SOA under different values of homogeneous linewidth: (a) Γ_h = 1 meV; (b) Γ_h = 5 meV; and (c) Γ_h = 20 meV. (Injection current density: J = 12 kA/cm^2, inhomogeneous broadening: Γ_{ih} = 50 meV). At t = 100 ps, a CW optical signal corresponding to the GS transition is injected into the active region. Simulations are terminated at T_s = 200 ps, and the time interval between consecutive plots in the time axes is 6 ps

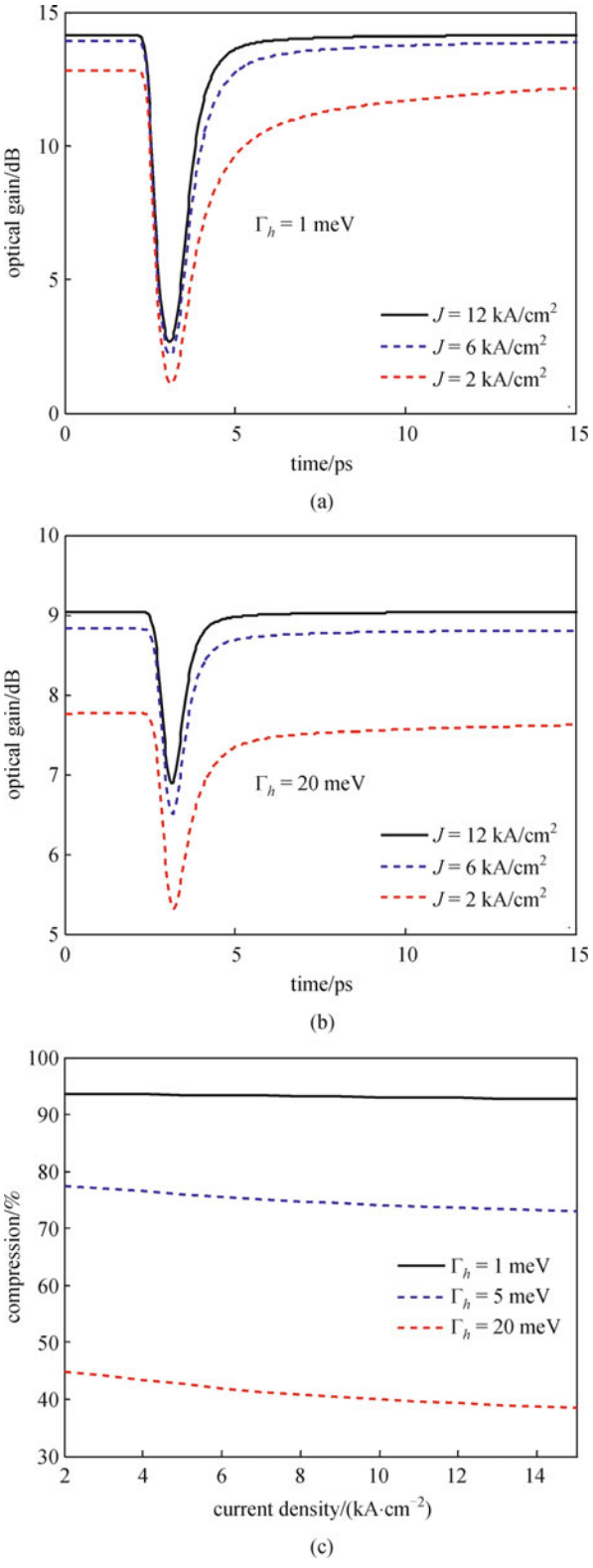

Fig. 5 Optical gain response of QD-SOA under different values of homogeneous linewidth: (a) Γ_h = 1 meV; and (b) Γ_h = 20 meV; (c) percentage of ultra-fast gain compression as function of current density for three different homogeneous linewidths. (Inhomogeneous linewidth: Γ_{ih} = 50 meV; pulse is injected at t = 3 ps; simulations are terminated at T_s = 15 ps)

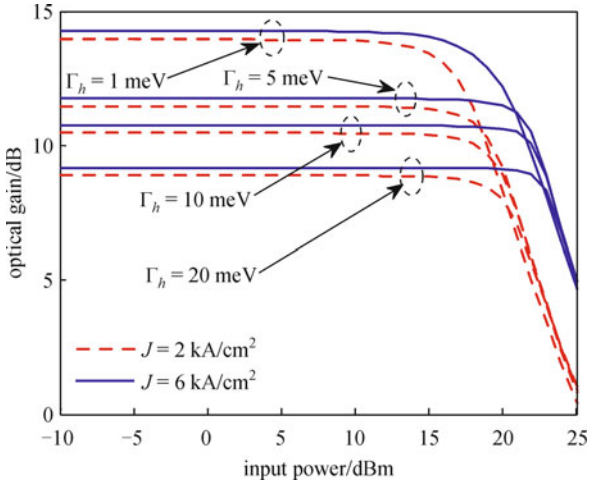

Fig. 6 Gain saturation curves of QD-SOA under different values of homogeneous linewidth (Γ_h = 1, 5, 10, 20 meV) and different current densities (J = 2, 6 kA/cm^2). Iinhomogeneous linewidth is Γ_{ih} = 50 meV in all curves

applications, where we need to reduce the injection current density and consequently the power losses.

To investigate the effect of homogeneous linewidth on the saturation power of the QD-SOA, the gain versus input power curves of the device for different homogeneous linewidths are plotted jointly in Fig. 6. It can be seen from the figure that the unsaturated optical gain of the QD-SOA increases with decreasing the homogeneous, while the saturation power of the amplifier decreases. For instant, with decreasing the homogeneous broadening from 20 to 1 meV, the saturation power becomes two times less. This is due to the fact that the numbers of QD groups participating to the amplification of the input signal decreases with decreasing the homogeneous linewidth. Consequently, a pronounced hole burning occurs at the energy of the input photons and saturation occurs for lower input powers. Therefore, for applications that a high saturation power is required, like booster amplifiers, the homogeneous linewidth should be large enough. On the other hand, for applications like nonlinear signal processing, the saturation power should be such that the SHB become the dominant saturation mechanism. Thus, a QD-SOA working at low temperature or having an undoped active region with well-confined QDs is appropriate for nonlinear signal processing applications [19].

4 Effects of inhomogeneous broadening on static and dynamic responses of QD-SOAs

Because of fluctuations in the size of self-assembled QDs and some variations in the shape of dots, the photoluminescence spectra of self-assembled QD-based active regions are inhomogeneously broadened. Experimental measurements have shown that the inhomogeneous linewidth of self-assembled InAs QDs is usually varied from 30 to 70 meV [22]. It has been proven that the inhomogeneous broadening affects the gain bandwidth as well as the gain and phase responses of QD-SOAs [12]. In this section, we investigate the effects of the inhomogeneous broadening on both static and dynamic characteristics of QD-SOAs. In Fig. 7(a), three inhomogeneous broadening functions and some homogenous broadening functions are presented. One can see that the number of QDs in each QD spectral group is dependent on the inhomogeneous lineshape. If the fluctuation in the size of QDs increases, the inhomogeneous linewidth increases, and vice versa. As can be seen in Figs. 7(b)–7(d), the gain spectrum of the QD ensemble is a function of both homogeneous and inhomogeneous broadening functions. The term $L_j^g G_j^s$ in Figs. 7(b)–7(d) is the product of the homogeneous and inhomogeneous broadening functions, which is proportional to the modal gain relevant to each QD group, is calculated for different inhomogeneous linewidths. We can see that with increasing the inhomogeneous broadening, the number of QD groups that participate to pulse amplification increases and the gain bandwidth increases. However, the modal gain per wavelength decreases as well.

To investigate the effect of the inhomogeneous broadening on dynamic response of QD-SOAs, similar to what we did in the previous section, we evaluate the response of the QD-SOA under different inhomogeneous linewidths. Simulation results are presented in Fig. 8, where the gain response of the QD-SOA is simulated under three different inhomogeneous linewidths. As can be seen in the figure, in all subfigures the GS steady-state is reached approximately after 40 ps. This time is similar to what we observed in Fig. 4. Also, as seen in the figure, the gain bandwidth is significantly reduced with decreasing the inhomogeneous broadening. Furthermore, the modal gain may be significantly enhanced through reducing the inhomogeneous linewidth. Figure 8 shows that with decreasing the inhomogeneous broadening from 75 to 25 meV, the maximum modal gain is doubled. In conclusion, while increasing the inhomogeneous linewidth increase the spectral width of the gain spectrum, a decrease in the modal gain in all range of the gain spectrum will be observed.

To investigate the effects of inhomogeneous broadening on the gain response of QD-SOAs, we numerically perform a single pulse pump-probe experiment, where a Gaussian shaped pulse is injected into the active region of the device. Simulation results are presented in Fig. 9. As can be seen in the figure, the optical gain is significantly enhanced for smaller inhomogeneous linewidths. Also, the gain compression increases as well. This behavior can be explained as follows. Once the magnitude of the inhomogeneous broadenings is small, a huge number of

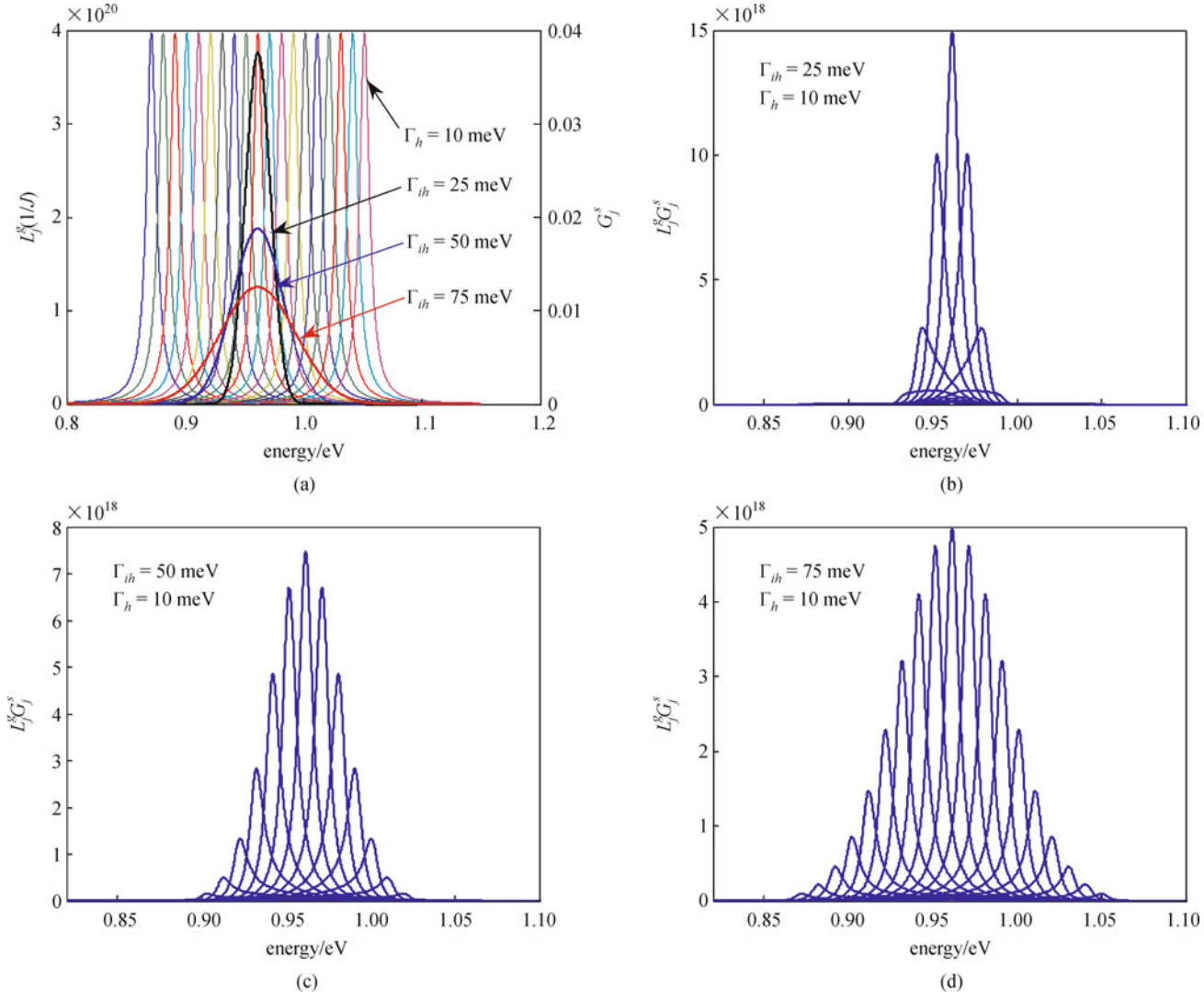

Fig. 7 (a) Homogenous and inhomogeneous broadening functions. The product of homogeneous and inhomogeneous functions ($L_j^g G_j^s$) for different inhomogeneous linewidths, (b) $\Gamma_{ih} = 25$ meV; (c) $\Gamma_{ih} = 50$ meV; and (d) $\Gamma_{ih} = 75$ meV. Homogeneous linewidth is $\Gamma_h = 10$ meV in all figures

the QDs contribute to the amplification of the input pulse. As a result, the optical gain of the QD-SOA increases and at the same time a strong hole burning occurs at the energy of the input photons.

A comparison between Figs. 9(a) and 9(b) reveals that the gain recovery time is approximately independent of the inhomogeneous linewidth. This is due to the fact that the ultrafast gain recovery is determined mainly by the carrier–carrier scattering processes which are functions of the injection current density. In addition, as seen from Fig. 9 (c), the gain compression is increased from less than 50% for $\Gamma_{ih} = 75$ meV to more the 90% for $\Gamma_{ih} = 25$ meV. This is due to enhancement of modal gain, which leads to a stronger carrier depletion and consequently a higher compression. The effect of inhomogeneous linewidth on the unsaturated optical gain as well as the saturation power can be seen in Fig. 10, where the gain saturation curves of the QD-SOA are plotted jointly for different values of the inhomogeneous linewidth. It can be seen from the figure that the unsaturated optical gain of the QD-SOA increases with decreasing the inhomogeneous linewidth. For instant, with decreasing the inhomogeneous broadening from 50 to 25 meV, the saturation power becomes three times less. Also, the saturation power of the amplifier decreases as well. This result is similar to what we obtained in Fig. 6. Thus, both homogeneous and inhomogeneous broadenings have almost parallel effects on the operation of QD-SOAs. Based on these results, for linear amplification purposes, the inhomogeneous linewidth should be large enough. Conversely, for optical processing purposes, the inhomo-

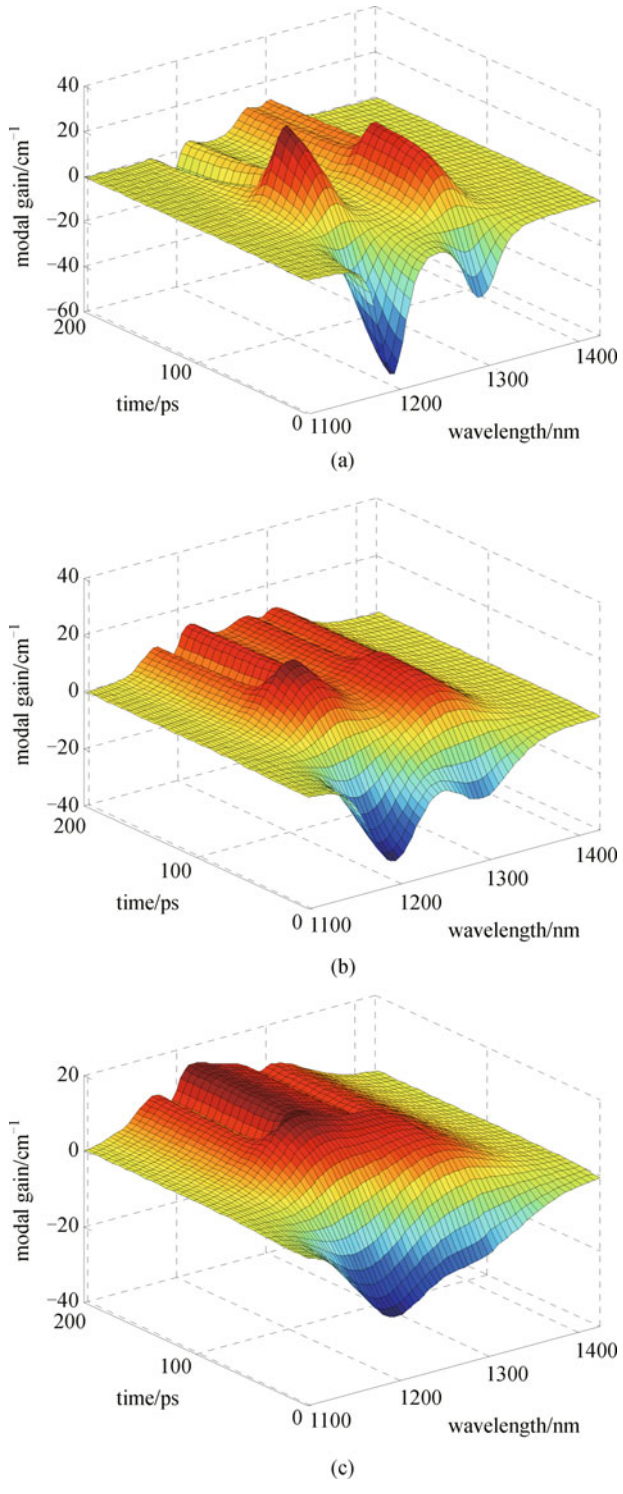

Fig. 8 Absorption/gain spectra of QD-SOA under three different inhomogeneous linewidths (a) Γ_{ih} = 25 meV; (b) Γ_{ih} = 50 meV; (c) Γ_{ih} = 75 meV. Pump current density is J = 12 kA/cm^2, and homogeneous broadening is Γ_h = 10 meV. At t = 100 ps, CW optical signal with photons energy corresponding to GS transition is injected into QD-SOA. Simulations are terminated at T_s = 200 ps, and the time interval between consecutive plots in the time axis is 6 ps

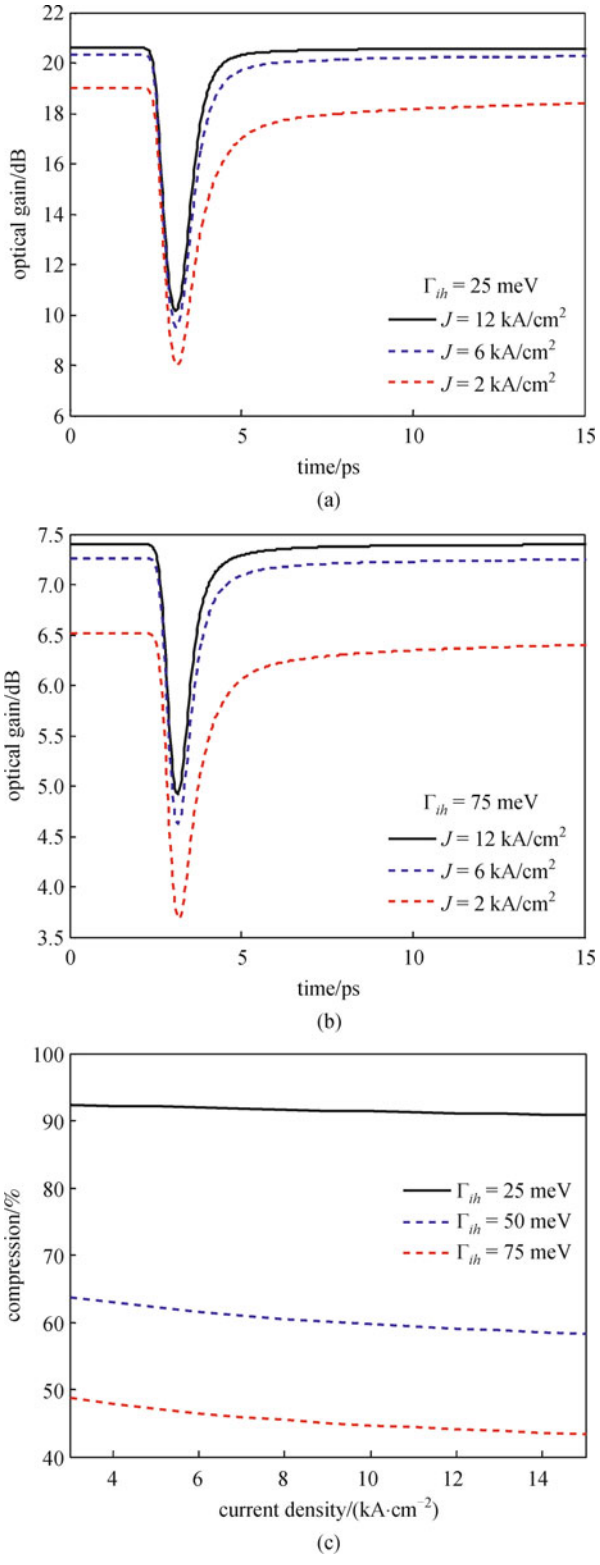

Fig. 9 Gain response of QD-SOA under different values of inhomogeneous linewidth and current density, (a) Γ_{ih} = 25 meV; and (b) Γ_{ih} = 75 meV; (c) percentage of ultra-fast gain compression as function of current density for different inhomogeneous linewidths. Homogeneous linewidth is Γ_h = 10 meV. Optical pulse is injected at t = 3 ps and simulations are terminated at T_s = 15 ps

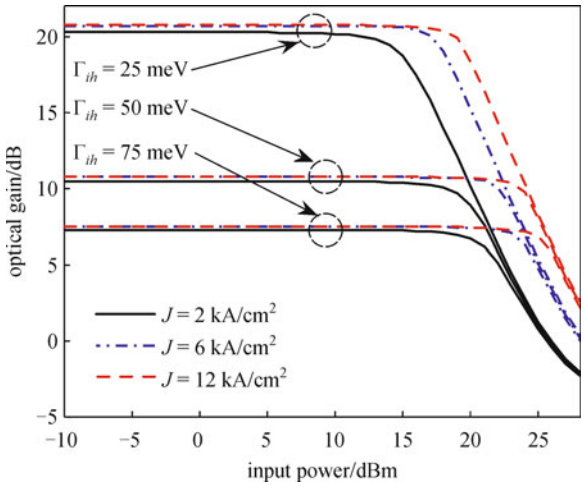

Fig. 10 Gain saturation curves of QD-SOA under different values of inhomogeneous broadening (Γ_{ih} = 25, 50, 75 meV) and different current densities (J = 2, 6, and 12 kA/cm^2). In all curves, the homogeneous linewidth is Γ_h = 10 meV

geneous linewidth should be as small as possible.

5 Conclusions

In this paper, the effects of homogeneous and inhomogeneous broadenings on the static and dynamic response of QD-SOAs were investigated. Simulation results showed that with decreasing the homogeneous broadening from 20 to 1 meV, the gain compression is increases from 40% to 90%, the unsaturated optical gain becomes approximately tripled, and the saturation power becomes two times less. Also, simulation results showed that with decreasing the inhomogeneous broadening from 50 to 25 meV, the gain compression increases from less than 50% to more than 90%, the unsaturated optical gain becomes approximately 10-fold, and the saturation power becomes three times less. We found out that the magnitude of the homogeneous and inhomogeneous linewidths should be optimized depends on the application of QD-SOAs. For nonlinear application, the homogeneous and inhomogeneous linewidths should be small enough to represent a strong nonlinearity. On the other hand, for linear amplification where a large saturation power is required, it is preferred to increase the homogeneous linewidth. The results of this paper are helpful for optimal design and fabrication of QD-SOAs for future all-optical networks.

References

1. Borri P, Langbein W, Hvam J M, Heinrichsdorff F, Mao H M, Bimberg D. Spectral hole-burning and carrier-heating dynamics in InGaAs quantum-dot amplifiers. IEEE Journal on Selected Topics in Quantum Electronics, 2000, 6(3): 544–551
2. Sugawara M, Ebe H, Hatori N, Ishida M, Arakawa Y, Akiyama T, Otsubo K, Nakata Y. Theory of optical signal amplification and processing by quantum-dot semiconductor optical amplifiers. Physical Review B: Condensed Matter and Materials Physics, 2004, 69(23): 235332
3. van der Poel M, Gehrig E, Hess O, Birkedal D, Hvam J M. Ultrafast gain dynamics in quantum-dot amplifiers: theoretical analysis and experimental investigations. IEEE Journal of Quantum Electronics, 2005, 41(9): 1115–1123
4. Kim J, Laemmlin M, Meuer C, Bimberg D, Eisenstein G. Theoretical and experimental study of high-speed small-signal cross-gain modulation of quantum-dot semiconductor optical amplifiers. IEEE Journal of Quantum Electronics, 2009, 45(3): 240–248
5. Bilenca A, Eisenstein G. On the noise properties of linear and nonlinear quantum-dot semiconductor optical amplifiers: the impact of inhomogeneously broadened gain and fast carrier dynamics. IEEE Journal of Quantum Electronics, 2004, 40(6): 690–702
6. Berg T W, Mørk J. Saturation and noise properties of quantum-dot optical amplifiers. IEEE Journal of Quantum Electronics, 2004, 40 (11): 1527–1539
7. Akiyama T, Ekawa M, Sugawara M, Kawaguchi K, Sudo H, Kuramata A, Ebe H, Arakawa Y. An ultrawide-band semiconductor optical amplifier having an extremely high penalty-free output power of 23 dBm achieved with quantum dots. IEEE Photonics Technology Letters, 2005, 17(8): 1614–1616
8. Meuer C, Schmeckebier H, Fiol G, Arsenijevi'c D, Kim J, Eisenstein G, Bimberg D. Cross-gain modulation and four-wave mixing for wavelength conversion in undoped and p-doped 1.3-m quantum dot semiconductor optical amplifiers. IEEE Journal of Photonics, 2010, 2(2): 141–151
9. Sugawara M, Hatori N, Ishida M, Ebe H, Arakawa Y, Akiyama T, Otsubo K, Yamamoto Y, Nakata Y. Recent progress in self-assembled quantum-dot optical devices for optical telecommunication: temperature-insensitive 10 Gb·s^{-1} directly modulated lasers and 40 Gb·s^{-1} signal-regenerative amplifiers. Journal of Physics D: Applied Physics, 2005, 38(13): 2126–2134
10. Rostami A, Nejad H B A, Qartavol R M, Saghai H R. Tb/s optical logic gates based on quantum-dot semiconductor optical amplifiers. IEEE Journal of Quantum Electronics, 2010, 46(3): 354–360
11. Meuer C, Kim J, Laemmlin M, Liebich S, Eisenstein G, Bonk R, Vallaitis T, Leuthold J, Kovsh A, Krestnikov I, Bimberg D. High-speed small-signal cross-gain modulation in quantum-dot semiconductor optical amplifiers at 1.3 μm. IEEE Journal on Selected Topics in Quantum Electronics, 2009, 15(3): 749–756
12. Kim J, Laemmlin M, Meuer C, Bimberg D, Eisenstein G. Effect of inhomogeneous broadening on gain and phase recovery of quantum-dot semiconductor optical amplifiers. IEEE Journal of Quantum Electronics, 2010, 46(11): 1670–1680
13. Kuntze S B, Zilkie A J, Pavel L, Aitchison J S. Nonlinear state-space model of semiconductor optical amplifiers with gain compression for system design and analysis. Journal of Lightwave Technology, 2008, 26(14): 2274–2281
14. Taleb H, Abedi K, Golmohammadi S. Operation of quantum-dot semiconductor optical amplifiers under nonuniform current injection. Applied Optics, 2011, 50(5): 608–617

15. Meuer C, Kim J, Laemmlin M, Liebich S, Capua A, Eisenstein G, Kovsh A R, Mikhrin S S, Krestnikov I L, Bimberg D. Static gain saturation in quantum dot semiconductor optical amplifiers. Optics Express, 2008, 16(11): 8269–8279
16. Xiao J L, Yang Y D, Huang Y Z. Investigation of gain recovery for InAs/GaAs quantum dot semiconductor optical amplifiers by rate equation simulation. Optical and Quantum Electronics, 2009, 41(8): 613–626
17. Vasileiadis M, Alexandropoulos D, Adams M J, Simos H, Syvridis D. Potential of InGaAs/GaAs quantum dots for applications in vertical cavity semiconductor optical amplifiers. IEEE Journal on Selected Topics in Quantum Electronics, 2008, 14(4): 1180–1187
18. Blood P. Gain and recombination in quantum dot lasers. IEEE Journal on Selected Topics in Quantum Electronics, 2009, 15(3): 808–818
19. Kim J, Laemmlin M, Meuer C, Bimberg D, Eisenstein G. Static gain saturation model of quantum-dot semiconductor optical amplifiers. IEEE Journal of Quantum Electronics, 2008, 44(7): 658–666
20. Ozgur G, Demir A, Deppe D G. Threshold temperature dependence of a quantum-dot laser diode with and without p-doping. IEEE Journal of Quantum Electronics, 2009, 45(10): 1265–1272
21. Wong H C, Ren G B, Rorison J M. Mode amplification in inhomogeneous QD semiconductor optical amplifiers. Optical and Quantum Electronics, 2006, 38(4–6): 395–409
22. Qasaimeh O. Optical gain and saturation characteristics of quantum-dot semiconductor optical amplifiers. IEEE Journal of Quantum Electronics, 2003, 39(6): 793–798